Supplementary Information

Se-Doped Sulfurized Polyacrylonitrile as a High-Performance Anode for Stable K-Ion Storage

Leqing Deng[ab]*, Lingjie Long[a], Lilin Chen[a], Yixian Xing[a], Jing Zheng[c]*, Qingxue Lai[d]*

[a]College of Environmental Science and Engineering, North China Electric Power University, Beijing, 102206, P. R. China

[b]Institute of Energy Power Innovation, North China Electric Power University, Beijing 102206, P. R. China

[c]Department of Chemistry and Materials Science, College of Science, Nanjing Forestry University, No. 159 Longpan Rd., Nanjing 210037, Jiangsu Province, P. R. China

[d]Jiangsu Key Laboratory of Electrochemical Energy Storage Technologies, College of Materials Science and Technology, Nanjing University of Aeronautics and Astronautics, Nanjing 210016, PR China

*Corresponding author: dengleqing@ncepu.edu.cn, jzheng62@njfu.edu.cn, laiqingxue@126.com

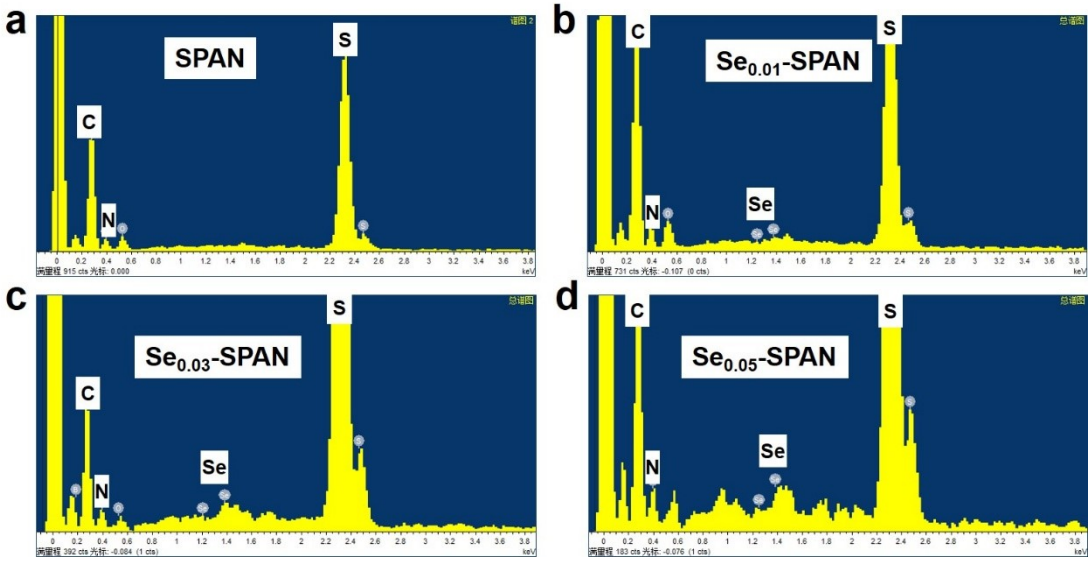

Figure S1. EDS results for (a) SPAN, (b) $Se_{0.01}$-SPAN, (c) $Se_{0.03}$-SPAN, and (d) $Se_{0.05}$-SPAN.

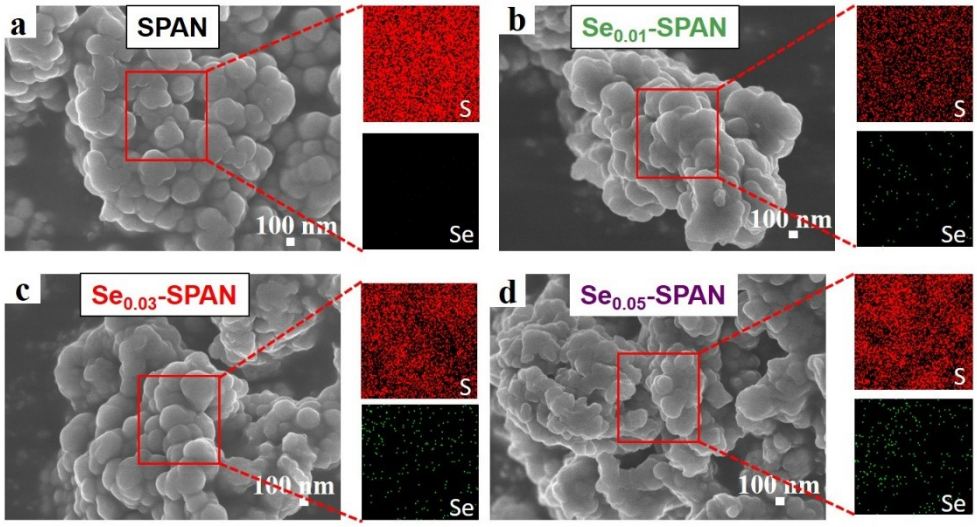

Figure S2. SEM image and corresponding EDS mapping images of S and Se elements for (a) SPAN, (b) $Se_{0.01}$-SPAN, (c) $Se_{0.03}$-SPAN, and (d) $Se_{0.05}$-SPAN.

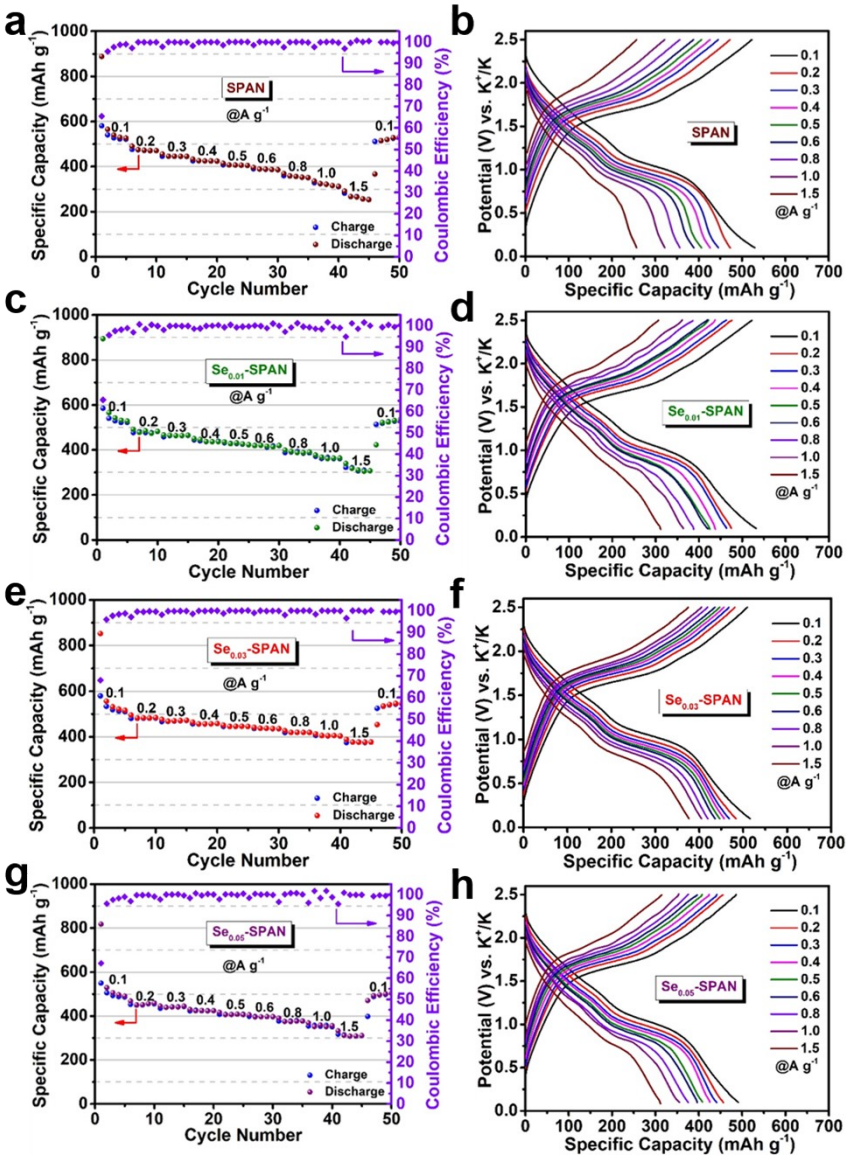

Figure S3. Rate capability and corresponding voltage profiles for (a, b) SPAN, (c, d) $Se_{0.01}$-SPAN, (e, f) $Se_{0.03}$-SPAN, and (g, h) $Se_{0.05}$-SPAN.

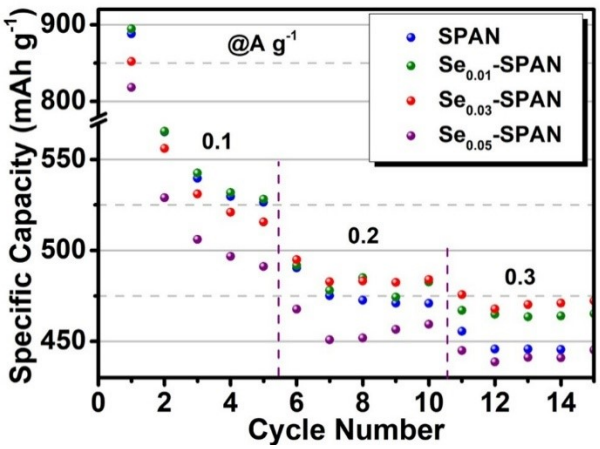

Figure S4. Rate capability of the samples within the currents of 0.1-0.3 A g^{-1}. The data are also shown in Figure 2a.

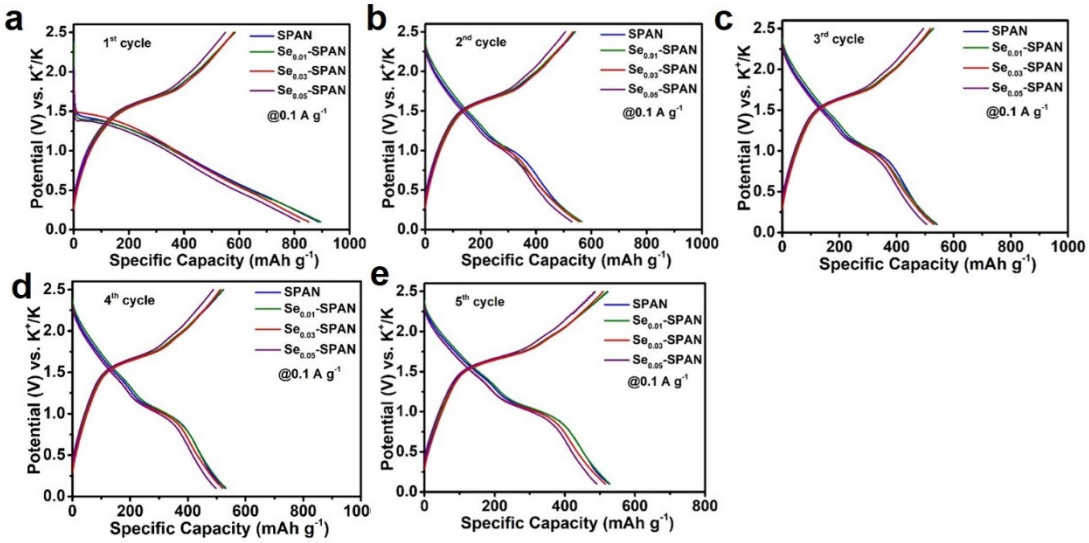

Figure S5. Voltage profiles of the four samples in the initial five cycles at 0.1 A g^{-1}: (a) the 1st cycle, (b) 2nd cycle, (c) 3rd cycle, (d) 4th cycle, and (e) 5th cycle.

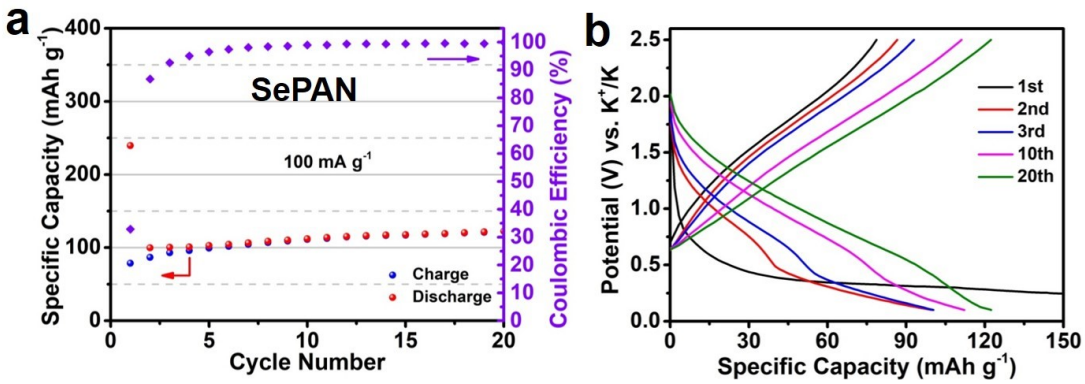

Figure S6. (a) Cycling performance and (b) corresponding voltage profiles for SePAN.

The selenide polyacrylonitrile SePAN was synthesized as that for SPAN but with Se and polyacrylonitrile as the raw materials. As shown in Figure S6, the as-obtained SePAN can only deliver the capacity of around 120 mAh $g_{(SePAN)}^{-1}$, which is far behind that of SPAN (~526.5 mAh $g_{(SPAN)}^{-1}$), demonstrating the poorly active Se species in SePAN. This can be seen as the negative effect of Se in SPAN-based materials.

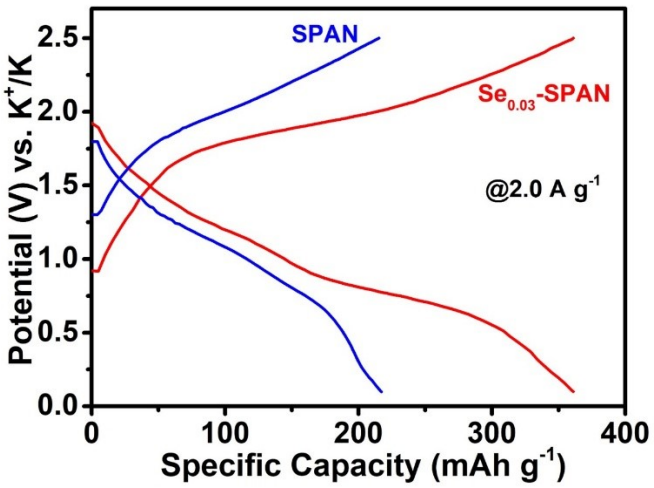

Figure S7. The voltage profiles of SPAN and $Se_{0.03}$-SPAN at 2.0 A g^{-1}.

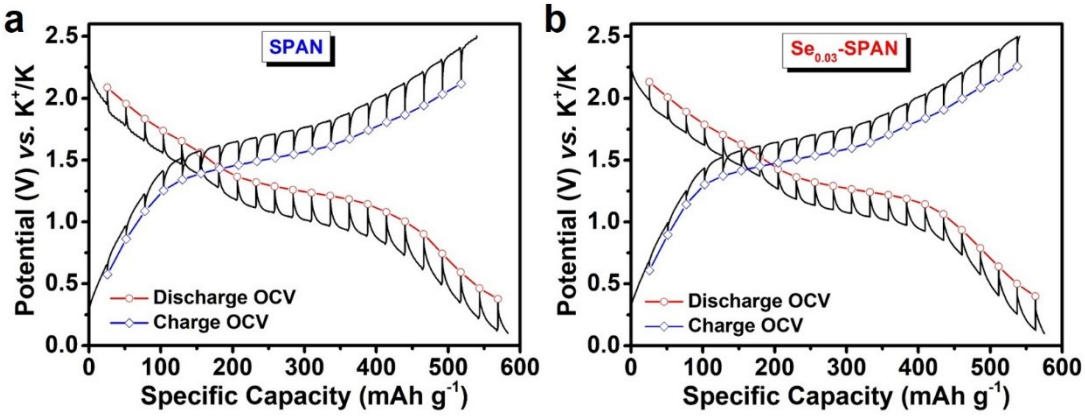

Figure S8. Quasi-equilibrium open-circuit-voltage (OCV) and transient voltage profiles for K-ion (de)intercalation in (a) SPAN and (b) $Se_{0.33}$-SPAN obtained from GITT.

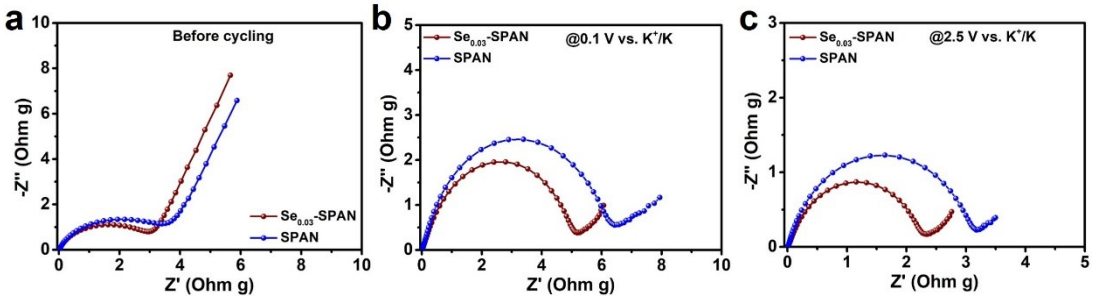

Figure S9. Nyquist plots of the SPAN and $Se_{0.03}$-SPAN electrodes before cycling (a) and at the states of 0.1 V (vs. K+/K) (b) and 2.5 V (vs. K+/K) (c).

As shown in Figure R9a, the pristine $Se_{0.03}$-SPAN delivers lower charge transfer resistance than SPAN. Similarly, compared to SPAN, $Se_{0.03}$-SPAN also shows lower charge transfer resistance at both the full discharge and full charge states (Figure S9b, c). The above EIS results demonstrate a better conductivity for $Se_{0.03}$-SPAN than SPAN.

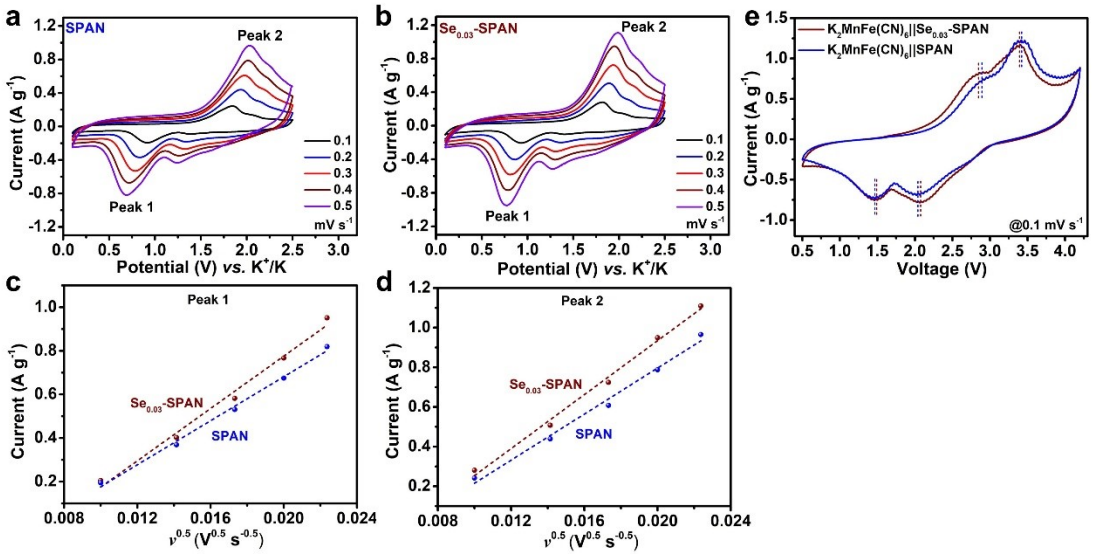

Figure S10. CV curves at different scan rates of (a) SPAN and (b) $Se_{0.03}$-SPAN. (c, d) The corresponding peak currents versus square root of scan rates (v) for SPAN and $Se_{0.03}$-SPAN: (c) Peak 1, (d) Peak 2. (e) The comparison of CV curves of $K_2MnFe(CN)_6$||SPAN and $K_2MnFe(CN)_6$||$Se_{0.03}$-SPAN full cells at a scan rate of 0.1 mV s^{-1}.

The kinetic mechanism for K^+ ion storage in SPAN and $Se_{0.03}$-SPAN was compared by the CV tests. As shown in Figure S10, in half cells, both SPAN and $Se_{0.03}$-SPAN maintain similar CV curves under increasing scan rates, suggesting a significant response capability to the scan rates. Figure S10c and S10d show the liner relationship between the peak currents and the square root of scan rates (v). The higher slope values for $Se_{0.03}$-SPAN for both Peak 1 and Peak 2 prove the augmented K^+ ion diffusion kinetics in $Se_{0.03}$-SPAN during the potassiation and depotassiation process, consistent with the GITT results. Therefore, the CV results in the half cells demonstrate an enhanced K-ion transfer kinetics after Se doping in SPAN material. As comparison in Figure S10e, the full cell with $Se_{0.03}$-SPAN anode also exhibits a smaller voltage hysteresis than the full cell with SPAN anode, signifying a faster K-ion transfer kinetics in $Se_{0.03}$-SPAN when compared to SPAN. Therefore, the CV results in the half and full cells demonstrate an enhanced K-ion transfer kinetics after Se doping in SPAN material.

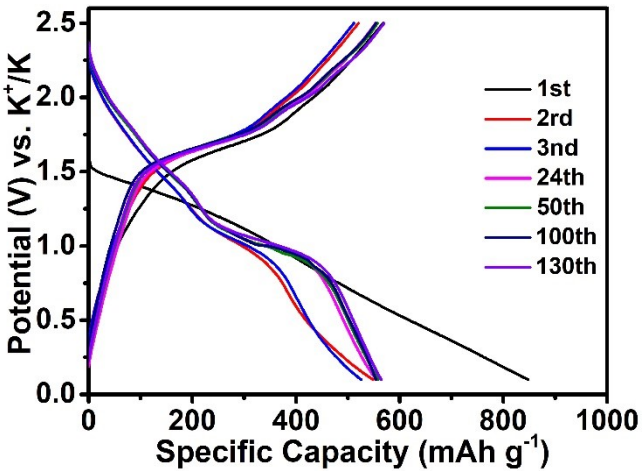

Figure S11. The voltage profiles of $Se_{0.03}$-SPAN at 0.1 A g^{-1}.

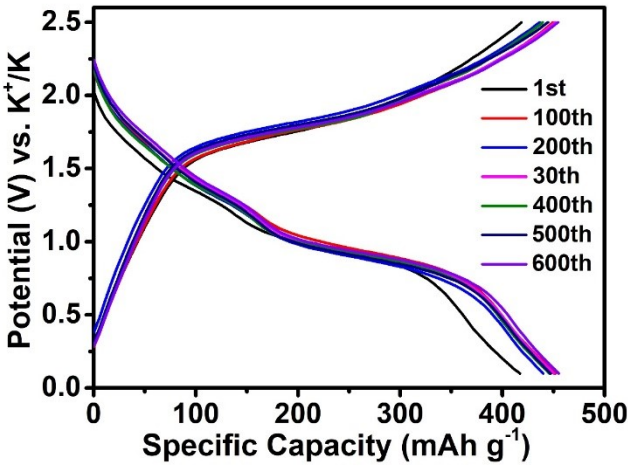

Figure S12. The voltage profiles of $Se_{0.03}$-SPAN at 0.5 A g^{-1}.

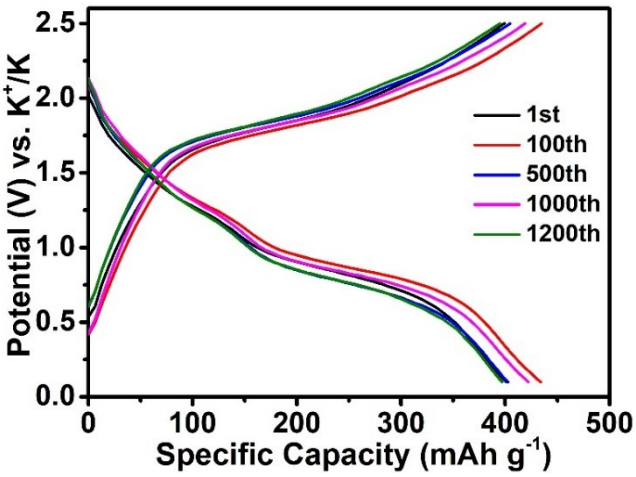

Figure S13. The voltage profiles of $Se_{0.03}$-SPAN at 1.0 A g^{-1}.

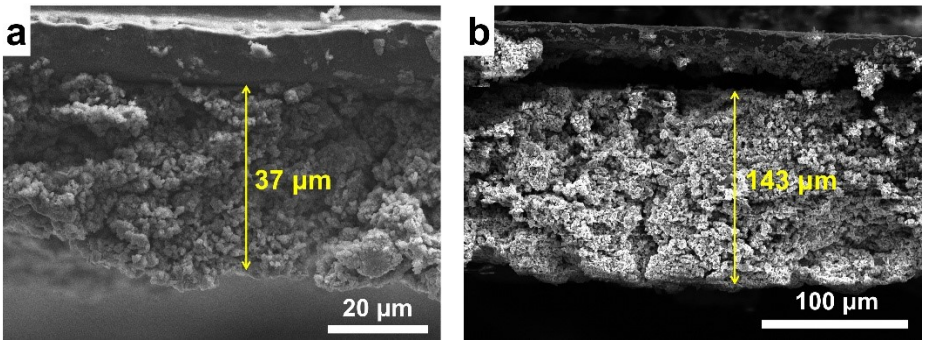

Figure S14. The thickness of the $Se_{0.03}$-SPAN electrode with the mass loading of (a) ~1 mg cm^{-2} and (b) ~4.2 mg cm^{-2}.

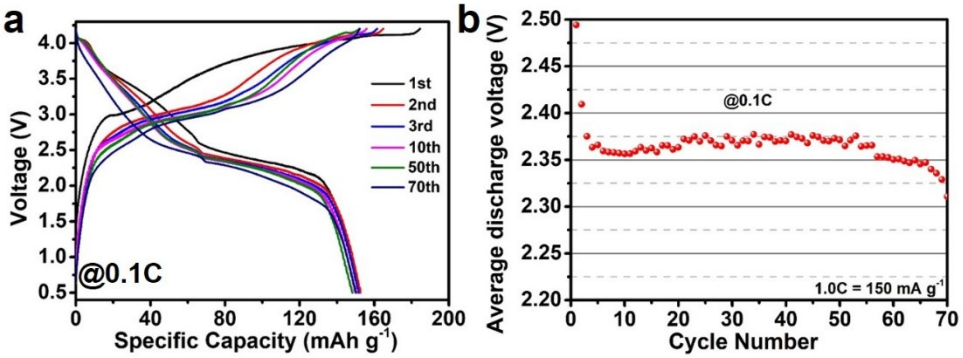

Figure S15. (a) Galvanostatic charge-discharge voltage profiles and (b) average discharge voltage of $K_2MnFe(CN)_6$||$Se_{0.03}$-SPAN full cell at 0.1 C.

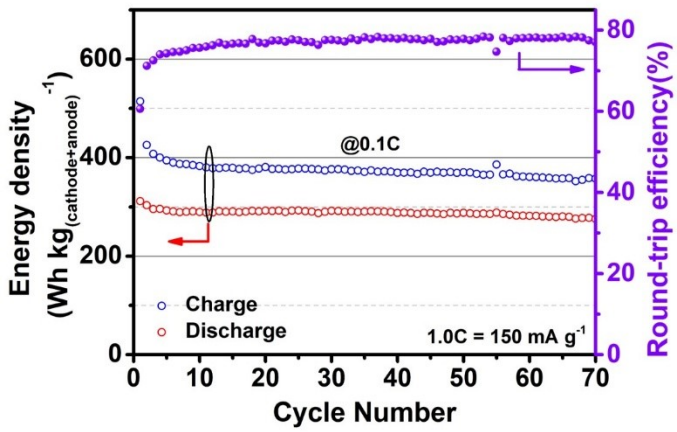

Figure S16. Energy density of the $K_2MnFe(CN)_6$||$Se_{0.03}$-SPAN full cell. The energy density is calculated based on the total mass of anode and cathode active materials in the full cell.

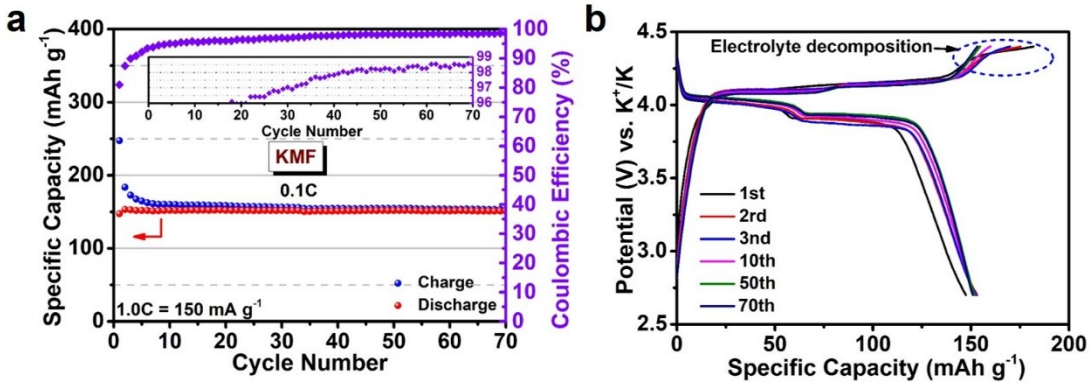

Figure S17. (a) The cycling stability and (b) corresponding voltage profiles of $K_2MnFe(CN)_6$ at 0.1C (1C = 150 mAh g^{-1}) in $K_2MnFe(CN)_6$||K half cell within the cathode potential range of 2.7-4.4 V (vs. K^+/K).

As shown in Figure S17a, the high-voltage $K_2MnFe(CN)_6$ cathode can only present the CE lower than 98.5% in $K_2MnFe(CN)_6$||K half cell at the current rate of 0.1C. Besides, the oxidative decomposition of the electrolyte can also be potently validated by the noticeable voltage tails at the end of charge process (Figure S17b). Consequently, the oxidative decomposition of the electrolyte limits the Coulombic efficiency in the full cells.

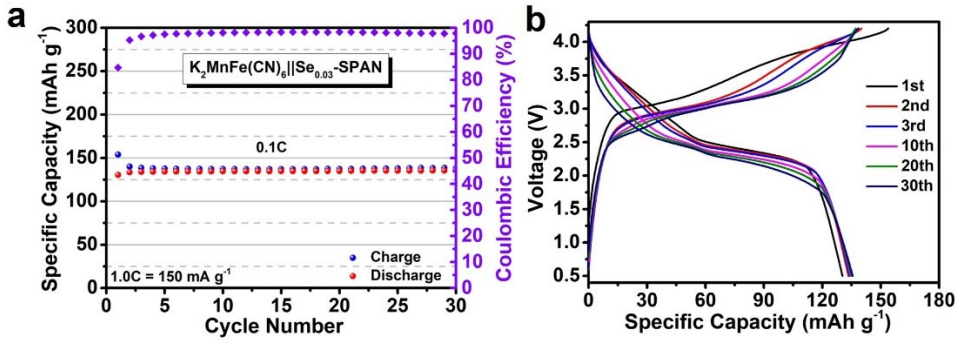

Figure S18. (a) Cycling stability and (b) corresponding voltage profiles of the $K_2MnFe(CN)_6$||$Se_{0.03}$-SPAN full cell at 0.1 C (calculated based on the mass of $K_2MnFe(CN)_6$ cathode). The mass loading of $Se_{0.03}$-SPAN anode is ~4.2 mg cm^{-2}.

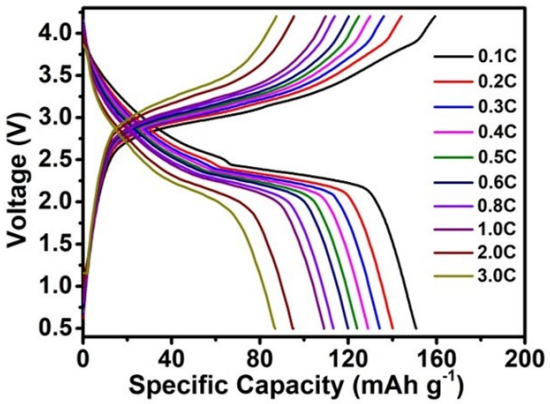

Figure S19. Voltage profiles of $K_2MnFe(CN)_6$||$Se_{0.03}$-SPAN full cell at varied current rates.

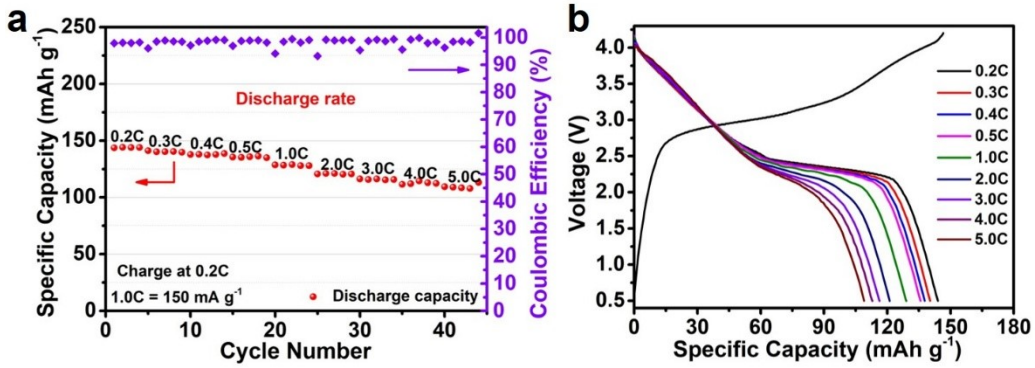

Figure S20. (a) Rate capability and (b) voltage profiles of $K_2MnFe(CN)_6$||$Se_{0.03}$-SPAN full cell under a constant charge current (0.2C) with different discharge currents from 0.2C to 5C.

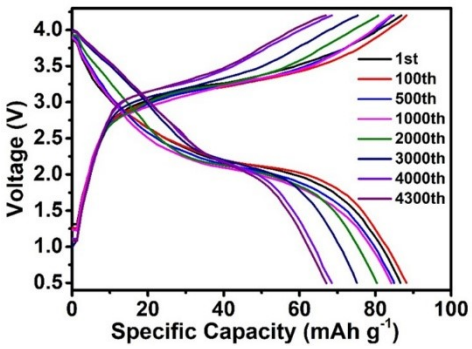

Figure S21. Voltage profiles of $K_2MnFe(CN)_6$||$Se_{0.03}$-SPAN full cell at 3C.

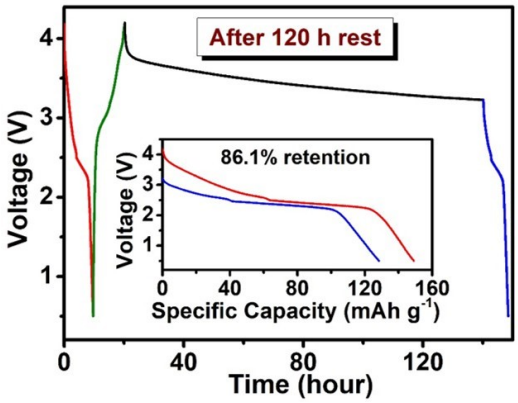

Figure S22. The voltage-time curve of the 120 h self-discharge process for $K_2MnFe(CN)_6$||$Se_{0.03}$-SPAN full cell. The inset is the comparison of the discharge behavior before and after the self-discharge process.

Table S1 Elemental analysis of SPAN and Se-doped SPAN.

Material	Element (wt%)				
	C	H	N	S	Se
SPAN	37.26	1.41	14.68	39.15	-
$Se_{0.01}$-SPAN	36.94	1.54	14.89	38.46	1.37
$Se_{0.03}$-SPAN	37.01	1.28	14.43	37.94	3.24
$Se_{0.05}$-SPAN	36.69	1.32	14.21	37.41	4.97

Table S2. Electrochemical performance of some reported anode materials for KIBs.

Materials	Potential range (V vs. K^+/K)	Reversible capacity (mAh g^{-1}) @current (A g^{-1})	Capacity retention (cycle number@current (A g^{-1}))	Rate capability (mAh g^{-1}) @current (A g^{-1})
$Se_{0.03}$-SPAN (This work)	0.1-2.5	556@0.1	100% (1200 cycles@1)	446@0.5 405.3@1 375.9@1.5
SPAN[1]	0.1-2.5	569@0.05	100% (1500 cycles@0.3)	416.8@0.5 326.2@1
Graphite[2]	0.01-2	270@139.5	100% (1000 cycles@0.558)	240@0.558 200@1.116
Hard carbon (HC)[3]	0.01-3	245@0.05	97% (50 cycles@0.1)	157@1 143@1.5
N-doped carbon nanofibers (NCNFs)[4]	0.01-3	~280@0.025	52% (100 cycles@0.2)	238@0.1 172@1
Bi@C[5]	0.01-1.5	466@0.02	74% (200 cycles@0.1)	413@0.1 340@0.4
BiNS/rGO[6]	0.1-1.5	338@0.05	80% (90 cycles@0.5)	320@1
Bi[7]	0.1-1.5	394.2@0.2	86.9% (300 cycles@0.8)	~350@0.8
SnS_x-N/P-CNFs (SnS-CNFs)[8]	0.01-3	468@0.1	92% (1000 cycles@0.2)	230@1
SnO_2@CF[9]	0.01-3	564.2@0.1	73% (400 cycles@1)	371.4@0.5 307.6@1
Sb@CSN[10]	0.01-2	223@0.05	95% (220 cycles@0.2)	214@0.1 200@0.2
P-COF@SWCNT (PCS)[11]	0.01-3	438@0.05	56% (1400 cycles@0.7)	199@0.5 158@1
P2[12]	0.1-2.5	268@0.66	66% (500 cycles@0.66)	240@1.3
K_2TP[13]	0.1-2	260@0.05	92% (100 cycles@0.2)	202@0.5 185@1

Table S3. Electrochemical performance of some reported K-ion full-cells.

Name	Positive|negative materials (mass ration)	Energy density (Wh kg^{-1})*	Cycle life (capacity retention@C-rate)
This work	$K_2MnFe[(CN)_6]$|$Se_{0.03}$-SPAN (1:0.3)	291.7	4000 (79.3%@3C) 4300 (77.5%@3C)
FC-1	$K_2MnFe[(CN)_6]$|S-PAN (1:0.3)[1]	290.9	2000 (81.1%@1C)
FC-2	$K_{1.94}Mn[Fe(CN)_6]_{0.994}$•$0.08H_2O$|Graphite (1:0.6)[14]	331.5	300 (98.5%@0.2C)
FC-3	$K_2FeFe(CN)_6$|Graphite (1:0.7)[2]	156	2500 (83.1%@11C)
FC-4	$K_2FeFe(CN)_6$|MCMB (1:0.67)[15]	118	600 (80%@3.9C)
FC-5	$K_2FeFe(CN)_6$|O,N co-doped carbon (1:0.5)[16]	238	4000 (~62%@10C)
FC-6	$K_{0.5}MnO_2$|Graphite (1:0.5)[17]	194.6	400 (83%@~4C)
FC-7	$K_{0.5}MnO_2$|Soft carbon (1:0.5)[18]	202.3	500 (82.5%@10C)
FC-8	$K_{0.77}MnO_2$•$0.23H_2O$|Hard-soft composite carbon (1.8:1)[19]	138.6	500 (80%@~7C)
FC-9	$K_{0.45}Mg_{0.1}Fe_{0.1}Mn_{0.8}O_2$|ESC-650 (1:0.33)[20]	80	200 (100%@0.2C)
FC-10	$KVPO_4F$|Graphite (1:1.33)[21]	122.4	200 (87.2%@0.67C)
FC-11	PTCDA|Graphite (1:0.6)[22]	88	100 (87%@~0.65C)

*The energy density is calculated based on the total mass of the cathode and anode materials in the full-cell.

References

1 L. Deng, Y. Hong, Y. Yang, J. Zhang, X. Niu, J. Wang, L. Zeng, W. Hao, L. Guo and Y. Zhu, *ACS Nano*, 2021, **15**, 18419–18428.

2 Y. Gao, X. Ma, Y. Yan, S. Zhang, J. Liang, B. Li, F. Kang and D. Zhai, *Adv. Energy Mater.*, 2025, **15**, 2404913.

3 Z. Yu, Q. Liu, C. Chen, Y. Zhu and B. Zhang, *J. Power Sources*, 2023, **557**, 232592.

4 Y. Xu, C. Zhang, M. Zhou, Q. Fu, C. Zhao, M. Wu and Y. Lei, *Nat. Commun.*, 2018, **9**, 1720.

5 J. Zheng, R. Chen, L. Nie, X. Chu, H. Wang, H. Xia, Y. Lin, Y. Li, Z. Lin, F. Xue, M. Ma and Q. Lai, *J. Colloid Interface Sci.*, 2025, **699**, 138164.

6 L. Zeng, M. Liu, P. Li, G. Zhou, P. Zhang and L. Qiu, *Sci. China Mater.*, 2020, **63**, 1920–1928.

7 K. Lei, C. Wang, L. Liu, Y. Luo, C. Mu, F. Li and J. Chen, *Angew. Chemie Int. Ed.*, 2018, **57**, 4687–4691.

8 Y. Wang, J. Liu, X. Chen, B. Kang, H.-E. Wang, P. Xiong, Q. Chen, M. Wei, N. Li, Q. Qian and L. Zeng, *Carbon N. Y.*, 2022, **189**, 46–56.

9 H. Qiu, L. Zhao, M. Asif, X. Huang, T. Tang, W. Li, T. Zhang, T. Shen and Y. Hou, *Energy Environ. Sci.*, 2020, **13**, 571–578.

10 J. Zheng, Y. Yang, X. Fan, G. Ji, X. Ji, H. Wang, S. Hou, M. R. Zachariah and C. Wang, *Energy Environ. Sci.*, 2019, **12**, 615–623.

11 X. Luo, W. Li, H. Liang, H. Zhang, K. Du, X. Wang, X. Liu, J. Zhang and X. Wu, *Angew. Chemie Int. Ed.*, 2022, **61**, e202117661.

12 V. Ramezankhani, A. Kozlov, E. V. Shchurik, S. Pluczyk-Małek, S. Vasil'ev, A. V. Mumyatov, M. Lapkowski, A. F. Shestakov and P. A. Troshin, *J. Power Sources*, 2023, **562**, 232744.

13 K. Lei, F. Li, C. Mu, J. Wang, Q. Zhao, C. Chen and J. Chen, *Energy Environ. Sci.*, 2017, **10**, 552–557.

14 L. Deng, J. Qu, X. Niu, J. Liu, J. Zhang, Y. Hong, M. Feng, J. Wang, M. Hu, L. Zeng, Q. Zhang, L. Guo and Y. Zhu, *Nat. Commun.*, 2021, **12**, 2167.

15 M. Gu, H. Fu, A. M. Rao, J. Zhou, Y. Lin, S. Wen, L. Fan and B. Lu, *Adv. Funct. Mater.*, 2024, **34**, 2407867.

16 Y. Wang, J. Zeng, Y. Wang, C. Zhang, Q. Wang, L. Gao, D. Sun, X. Jiang, M. Hu, L. Yang, D. Xie, Y. Hao, Z. Hu and X. Wang, *Adv. Mater.*, 2024, **36**, 2410132.

17 L. Deng, T. Wang, Y. Hong, M. Feng, R. Wang, J. Zhang, Q. Zhang, J. Wang, L. Zeng, Y. Zhu and L. Guo, *ACS Energy Lett.*, 2020, **5**, 1916–1922.

18 S. Zhao, G. Li, B. Zhang, S. Zhang, Y. Liu, J. Zhou, M. Luo and S. Guo, *Adv. Mater.*, 2024, **36**, 2405184.

19 B. Lin, X. Zhu, L. Fang, X. Liu, S. Li, T. Zhai, L. Xue, Q. Guo, J. Xu and H. Xia, *Adv. Mater.*, 2019, **31**, 1900060.

20 Z. Wu, S. Xu, Z. Lu, L. Chen, Y. Liang, L. Wang, T. Wei, D. Zhang and R. Li, *Carbon N. Y.*, 2025, **243**, 120509.

21 Y. Gao, W. Li, B. Ou, S. Zhang, H. Wang, J. Hu, F. Kang and D. Zhai, *Adv. Funct. Mater.*, 2023, **33**, 2305829.

22 Q. Feng, J. Jiang, S. Li, G. Zhou, X. Kong, Y. Chen, Q. Zhuang and Z. Ju, *Small*, 2025, **21**, 2406506.